Okano, T., Nakagawa, T., Endo, T., Kim, T.S., Kita, T., Tamura, T., Matsumoto, M., Ohno, T., Sakamoto, T., Iguchi, F. & Ito, J. (2005) Engraftment of embryonic stem cell-derived neurons into the cochlear modiolus. *Neuroreport*, **16**, 1919–1922.

Olivius, P., Alexandrov, L., Miller, J.M., Ulfendahl, M., Bagger-Sjoback, D. & Kozlova, E.N. (2004) A model for implanting neuronal tissue into the cochlea. *Brain Res. Brain Res. Protoc.*, **12**, 152–156.

Pal, B., Por, A., Szucs, G., Kovacs, I. & Rusznak, Z. (2003) HCN channels contribute to the intrinsic activity of cochlear pyramidal cells. *Cell. Mol. Life Sci.*, **60**, 2189–2199.

Pollock, K., Stroemer, P., Patel, S., Stevanato, L., Hope, A., Miljan, E., Dong, Z., Hodges, H., Price, J. & Sinden, J.D. (2006) A conditionally immortal clonal stem cell line from human cortical neuroepithelium for the treatment of ischemic stroke. *Exp. Neurol.*, **199**, 143–155.

Regis, J., Pellet, W., Delsanti, C., Dufour, H., Roche, P.H., Thomassin, J.M., Zanaret, M. & Peragut, J.C. (2002) Functional outcome after gamma knife surgery or microsurgery for vestibular schwannomas. *J. Neurosurg.*, **97**, 1091–1100.

Renfranz, P.J., Cunningham, M.G. & McKay, R.D. (1991) Region-specific differentiation of the hippocampal stem cell line HiB5 upon implantation into the developing mammalian brain. *Cell*, **66**, 713–729.

Rubel, E.W. & Fritzsch, B. (2002) Auditory system development: primary auditory neurons and their targets. *Annu. Rev. Neurosci.*, **25**, 51–101.

Ryu, M.Y., Lee, M.A., Ahn, Y.H., Kim, K.S., Yoon, S.H., Snyder, E.Y., Cho, K.G. & Kim, S.U. (2005) Brain transplantation of neural stem cells cotransduced with tyrosine hydroxylase and GTP cyclohydrolase 1 in Parkinsonian rats. *Cell Transplant*, **14**, 193–202.

Sakamoto, T., Nakagawa, T., Endo, T., Kim, T.S., Iguchi, F., Naito, Y., Sasai, Y. & Ito, J. (2004) Fates of mouse embryonic stem cells transplanted into the inner ears of adult mice and embryonic chickens. *Acta Otolaryngol.* **124** (Suppl.), 48–52.

Samii, M. & Matthies, C. (1997) Management of 1000 vestibular schwannomas (acoustic neuromas): hearing function in 1000 tumor resections. *Neurosurgery*, **40**, 248–260.

Sartiani, L., Bochet, P., Cerbai, E., Mugelli, A. & Fischmeister, R. (2002) Functional expression of the hyperpolarization-activated, non-selective cation current I (f) in immortalized HL-1 cardiomyocytes. *J. Physiol.*, **545**, 81–92.

Sekiya, T., Hatayama, T., Shimamura, N. & Suzuki, S. (2000) An *in vivo* quantifiable model of cochlear neuronal degeneration induced by central process injury. *Exp. Neurol.*, **161**, 490–502.

Sekiya, T., Kojima, K., Matsumoto, M., Kim, T.S., Tamura, T. & Ito, J. (2006) Cell transplantation to the auditory nerve and cochlear duct. *Exp. Neurol.*, **198**, 12–24.

Starr, A., Picton, T.W., Sininger, Y., Hood, L.J. & Berlin, C.I. (1996) Auditory neuropathy. *Brain*, **119**, 741–753.

Stone, J.S. & Rubel, E.W. (2000) Temporal, spatial, and morphologic features of hair cell regeneration in the avian basilar papilla. *J. Comp. Neurol.*, **417**, 1–16.

Szabo, Z.S., Harasztosi, C.S., Sziklai, I., Szucs, G. & Rusznak, Z. (2002) Ionic currents determining the membrane characteristics of type I spiral ganglion neurons of the guinea pig. *Eur. J. Neurosci.*, **16**, 1887–1895.

Tamura, T., Nakagawa, T., Iguchi, F., Tateya, I., Endo, T., Kim, T.S., Dong, Y., Kita, T., Kojima, K., Naito, Y., Omori, K. & Ito, J. (2004) Transplantation of neural stem cells into the modiolus of mouse cochleae injured by cisplatin. *Acta Otolaryngol*, **124** (Suppl.), 65–68.

Tardy, M. (2002) Role of laminin bioavailability in the astroglial permissivity for neuritic outgrowth. *An Acad. Bras Cienc*, **74**, 683–690.

Vincent, V.A., Robinson, C.C., Simsek, D. & Murphy, G.M. (2002) Macrophage colony stimulating factor prevents NMDA-induced neuronal death in hippocampal organotypic cultures. *J. Neurochem.*, **82**, 1388–1397.

Virley, D., Ridley, R.M., Sinden, J.D., Kershaw, T.R., Harland, S., Rashid, T., French, S., Sowinski, P., Gray, J.A., Lantos, P.L. & Hodges, H. (1999) Primary CA1 and conditionally immortal MHP36 cell grafts restore conditional discrimination learning and recall in marmosets after excitotoxic lesions of the hippocampal CA1 field. *Brain*, **122**, 2321–2335.

Winkler, C., Kirik, D. & Bjorklund, A. (2005) Cell transplantation in Parkinson's disease: how can we make it work? *TINS*, **28**, 86–92.

The potential use of bone marrow stromal cells for cochlear cell therapy

Sadia Sharif[a,c], Takayuki Nakagawa[a], Tsunehisa Ohno[a], Masahiro Matsumoto[a], Tomoko Kita[a,b], Sheikh Riazuddin[c] and Juichi Ito[a]

[a]Department of Otolaryngology-Head and Neck Surgery, Kyoto University Graduate School of Medicine, [b]Organogenesis and Neurogenesis Group, Center for Developmental Biology, RIKEN, Kobe, Japan and [c]National Center of Excellence in Molecular Biology, University of the Punjab, Pakistan

Correspondence to Dr Takayuki Nakagawa, MD, PhD, Department of Otolaryngology-Head and Neck Surgery, Graduate School of Medicine, Kyoto University, Kawaharacho 54, Shogoin, Sakyo-ku, 606-8507 Kyoto, Japan
Tel: +81 75 751 3346; fax: +81 75 751 7225; e-mail: tnakagawa@ent.kuhp.kyoto-u.ac.jp

Received 10 October 2006; accepted 25 November 2006

This study investigated the potential of bone-marrow stromal cell transplantation for cell replacement therapy in the cochlea. Bone-marrow stromal cells labeled with enhanced green fluorescent protein were injected into the perilymphatic space of normal cochleae in mice. Histological analysis 2 weeks after transplantation demonstrated that transplanted cells settled within the cochlear tissues, especially in the spiral ligament and the spiral limbus, although most transplants were located in the perilymphatic space. Some of the transplanted cells expressed the cochlear gap-junction protein connexin 26. These findings indicate the potential of bone-marrow stromal cells for delivering therapeutic molecules and for the restoration of cochlear cells, particularly in the spiral ligament and the spiral limbus. *NeuroReport* 18:351–354

Keywords: bone-marrow stromal cell, cell therapy, cochlea, migration, transplantation

Introduction

Treatment options for sensorineural hearing loss (SNHL) are currently limited to cochlear implants and hearing aids. Hence, there is a requirement for alternative means of biological therapy, including cell and/or gene therapy. Indeed, recent studies have indicated that cell or gene therapy could be utilized to regenerate hair cells [1,2] and neurons [3] in the inner ear, and to deliver therapeutic molecules to the inner ear [4–6]. More recently, transplantation of gene-transfected cells has been reported as an efficient strategy to deliver genes into the inner ear [7].

Bone-marrow stromal cells (BMSCs) are possible candidates for transplants for cell therapy for the treatment of SNHL. They have the potential for differentiation into various types of cells and are easily obtained from one's own bone marrow. In addition, BMSCs are capable of secretion of several growth factors [8], which are included in cochlear protectants [9–11]. BMSC transplantation, therefore, could be utilized in three different strategies for inner ear treatment, restoration of missing cells, providing growth factors and delivering genes. In this study, we examined the distribution and characteristics of BMSCs after transplantation into cochleae of C57BL/6 mice to evaluate the potential of BMSCs as a source of cells for cell-replacement-therapy for the cochlea.

Materials and methods

Animals

Male C57BL/6 mice (n=6, SLC Japan, Hamamatsu, Japan) aged 10 weeks were used as the recipients. The experimental protocols were approved by the Animal Research Committee of Kyoto University Graduate School of Medicine, and were conducted in accordance with the US National Institutes of Health Guidelines for the Care and Use of Laboratory Animals.

Bone-marrow stromal cells

The BMSCs were obtained from enhanced green fluorescent protein (GFP)-transgenic mice [strain B6;C3-*Tg(ACtb-EGFP)CX-FM139Osb*] [12]. Under general anesthesia with ketamine (75 mg/kg) and xylazine (9 mg/kg), the tibias and femurs of the animals (n=4) were collected, and the medullary cavity was aspirated to harvest the bone marrow. The BMSCs were cultured in a 25-cm^2 flask with 8 ml of Iscove's modified Dulbecco's medium (Invitrogen, Carlsbad, California, USA) supplemented with 20% fetal bovine serum (Thermo Trace, Victoria, Australia), 100 U/ml of penicillin (Nacalai Tesque Inc., Kyoto, Japan) and 100 µg/ml of streptomycin (Nacalai Tesque Inc.). The cells were cultured at 37°C under 5% CO_2. The medium was changed twice weekly until the cells were 80% confluent. Non-adherent cells were removed during the medium-change procedure and the adherent cells were collected. After two passages, the cells were suspended in Iscove's modified Dulbecco's medium at a concentration of 1×10^5 cells/µl.

Transplantation

Cell transplantation was performed under general anesthesia with ketamine and xylazine. A retroauricular incision was made in the left ear of each mouse and the otic bulla

was exposed. The bony wall of the bulla was partially resected to expose the basal turn of each cochlea. A small perforation was then made in the lateral wall at the basal turn of the cochlea corresponding to the location of the scala tympani (ST). Cell suspensions of GFP-labeled BMSCs (2 μl; 10^5 cells/μl) were injected through a fine glass needle using a microinfusion pump. Subsequently, the perforation was plugged with a fat graft and covered with fibrin glue.

Histology

Under general anesthesia, the animals were transcardially perfused with phosphate-buffered saline at pH 7.4, followed by 4% paraformaldehyde in phosphate buffer at pH 7.4 on day 14. The temporal bones were immediately dissected out and immersed in the same fixative for 4 h at 4°C. After decalcification, cryostat sections (8 μm thickness) were cut and immunohistochemical analysis for GFP, CD43, nestin, β-III-tubulin, E-cadherin and Cx26 was performed. BMSCs grown on sterile cover glasses were also subjected to immunocytochemical analysis to determine the characteristics of the BMSCs before transplantation. Anti-GFP mouse monoclonal (1:200; Invitrogen, San Diego, California, USA) or rabbit polyclonal (1:500, Molecular probes, Eugene, Oregon, USA), anti-CD43 rat monoclonal (1:200; Pharmingen, San Diego, California, USA), anti-nestin rat monoclonal (1:200; Pharmingen), anti-β-III-tubulin mouse monoclonal (1:500, Covance Research Products, Berkeley, California, USA), anti-Cx26 rabbit polyclonal (1:500; Zymed, San Francisco, California, USA) and anti-E-cadherin mouse monoclonal antibody (1:200; Takara Bio, Otsu, Japan) were used as the primary antibodies. The secondary antibody was Alexa-546 or 488-conjugated anti-mouse, rat or rabbit antibody (1:400; Molecular Probes). Counterstaining by 4′,6-diamidino,2-phenylindole dihydrochloride (DAPI; 1 μg/ml in phosphate-buffered saline; Molecular Probes) was performed at the end of the staining procedures. Specimens stained without primary antibodies served as negative controls. Cryostat-sections of mouse cerebellum on embryonic day 12 were used as positive controls for nestin. The specimens were viewed with a Nikon Eclipse E600 fluorescence microscope (Nikon, Tokyo, Japan) or a Leica TCS-SP2 confocal laser-scanning microscope (Leica Microsystems, Tokyo, Japan).

Four mid-modiolar sections were chosen from each cochlea and subjected to quantitative analysis of the number of transplanted cells in the cochlea. We counted the number of cells expressing both GFP and DAPI as transplant-derived cells. The distribution of the engrafted cells was divided into four compartments: the scala vestibuli (SV), the scala media, the ST and the cochlear tissues. In addition, the cochlear tissues were further subdivided into three compartments: the spiral ligament (SL), the spiral limb (SLB) and the other components of the cochleae. The number of transplant-derived cells expressing CD34, nestin or Cx26 was also counted in four sections from each cochlea. The expression ratio for each marker was then determined by dividing the numbers of transplant-derived cells expressing each marker by those of transplant-derived cells in each section. The average in four sections was defined as the data for the cochlea. The expression ratios for these markers were also calculated using four samples of BMSCs grown on sterile cover glasses. All the data were represented by the means and the standard deviations.

Statistics

Statistical analyses for the location of BMSC-derived cells in the cochlea were performed using one-way analysis of variance followed by the Scheffe's test. The unpaired *t*-test was used in analyses of the expression ratios for CD34, nestin and Cx26. A P value <0.05 was considered statistically significant.

Results

BMSC-derived cells labeled with GFP were found in all the transplanted cochleae (Fig. 1a). The mean number of GFP-positive cells in one mid-modiolar section per cochlea was 180 ± 38 ($n=6$). The transplanted cells were distributed from the base to the apex of the cochleae. No apparent difference in distribution of transplanted cells was found among the turns of cochleae. BMSC-derived cells were predominantly located in the perilymphatic space of the cochleae: $67.3 \pm 7.3\%$ in the ST and $18.1 \pm 10.8\%$ in the SV (Fig. 1b). The ST was the region in which BMSC-derived cells were most frequently observed. BMSC-derived cells were also observed within the cochlear tissues ($12.8 \pm 9.2\%$), indicating the migration activity of BMSCs into various parts of the cochleae. Of BMSC-derived cells located in cochlear tissues, $57.4 \pm 8.0\%$ were found in the SL (Fig. 1b–d) and $17.3 \pm 3.4\%$ were found in the SLB (Fig. 1b, e, p and s). In addition, cell aggregates of transplants that were located in the perilymphatic space were adjacent to those located in the SL (Fig. 1c and d). Within the SLB, the transplanted cells were located in the medial region, which faced the SV (Fig. 1e, p and s). BMSC-derived cells were also observed in other compartments of the cochleae: the sensory epithelium (Fig. 1f and g), the osseous spiral lamina (Fig. 1e and f) and the acoustic nerve (Fig. 1h).

Before transplantation, $74.2 \pm 17.6\%$ of the BMSCs expressed CD34 (Fig. 1i–k) and $3.5 \pm 2.0\%$ were immunoreactive for nestin (Fig. 1l–n). No immunoreactivity for the other markers used in this study was identified in the BMSCs before transplantation. Two weeks after transplantation into the cochleae, CD34-positive transplants were found (Fig. 1p–r); however, the expression ratio for CD34 in the BMSC-derived cells had significantly decreased to $7.3 \pm 8.3\%$ (Fig. 1o, $P=0.0003$). Immunoreactivity for nestin was still detected, but was significantly reduced to $0.9 \pm 0.8\%$ (Fig. 1o, $P=0.04$). Cx26 expression was detected in $4.7 \pm 2.7\%$ of the BMSC-derived cells that had settled in the cochleae (Fig. 1o, s–u). The difference in the ratio of Cx26 expression between before and after transplantation was significant at $P=0.02$. By contrast, immunoreactivity for E-cadherin and β-III-tubulin was not found in these cells.

Discussion

We hypothesized that BMSC transplantation could be utilized in three different strategies for inner ear treatment, restoration of missing cells, providing growth factors and delivering genes. These findings demonstrate that BMSCs can survive in various parts of the cochleae after injection into the perilymphatic space of cochleae, indicating possible use of BMSC transplantation for providing growth factors in the cochlea. These results, however, demonstrated significant decrease of the rate for CD34 expression in BMSC-derived cells in cochleae in comparison with that in BMSCs before transplantation, indicating maturation

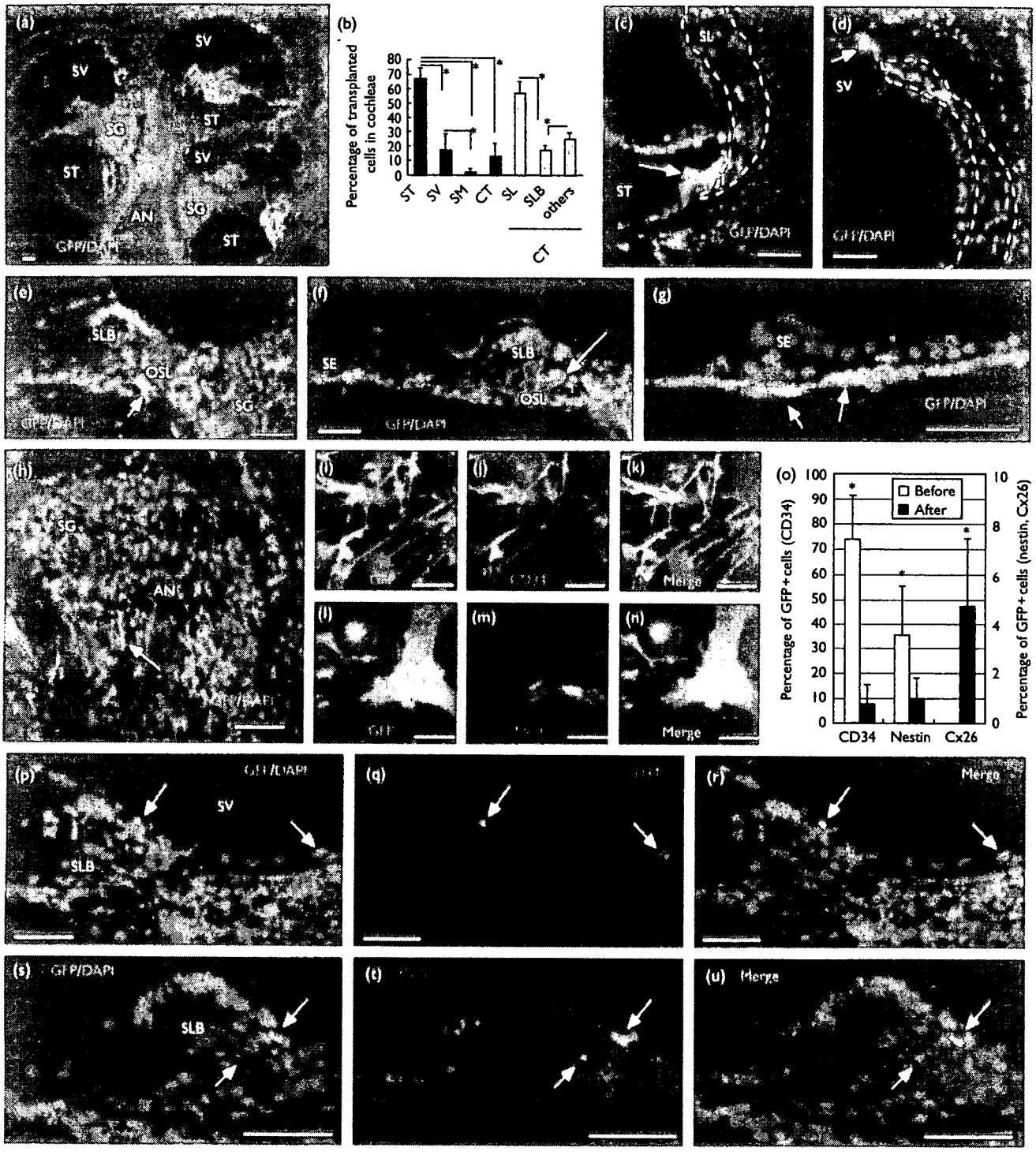

Fig. 1 Distribution of engrafted bone-marrow stromal cells in the cochlea and the expression of cell markers before and after transplantation. Transplanted cells expressing green fluorescent protein (GFP) were observed from the base to the apex of the cochleae, and were mainly located in the scala tympani (ST) and the scala vestibuli (SV) (a). Among the cochlear compartments, the transplanted cells were most frequently found in the ST (analysis of variance with the Scheffe's test, $*P<0.05$ in b) and in cochlear tissue (CT), the spiral ligament (SL) is the site in which transplanted cells were most frequently observed (b). Some of the transplanted cells in the ST (arrow in c) or the SV (arrow in d) were located adjacent to the SL (indicated by the dotted lines in c, d) in which transplanted cells were found. Transplanted cells were also observed in the spiral limb (SLB) (e, p, s), the osseous spiral lamina (OSL) (arrow in e, f), the sensory epithelium (SE) (asterisk in f, g), the connective tissue beneath the SE (arrows in g) and the acoustic nerve (AN) (arrow in h). Before transplantation, the BMSCs expressed CD34 (i–k) and a few were positive for nestin expression (l–n). The ratio of CD34 or nestin expression was significantly reduced after transplantation (unpaired *t*-test, $*P<0.05$ in o), and that of connexin26 (Cx26) expression was significantly increased after transplantation (o, the *y*-axis on the right side shows percentage for the CD34 ratio and the left for the ratio of nestin or Cx26). The transplanted cells that settled in the SV exhibited the expression of CD34 (arrows in p–r), and those in the SLB showed Cx26 expression (arrow in s–u). The scale bars represent 50 μm. Bars in b and o show standard deviations.

of BMSCs after transplantation. It is unclear whether BMSC-derived cells in the cochlea preserve the capability for secretion of growth factors displayed by BMSCs before transplantation [8]. Therefore, the potential of BMSC-derived cells in the cochlea for the secretion of growth factors should be examined to determine the ability of application of growth factors in the cochlea by BMSC transplantation.

Previously, we have demonstrated the delivery of a secreting protein to the inner ear by transplanting genetically manipulated fibroblasts without using virus vectors [7]. The fibroblasts were, however, distributed throughout the perilymphatic space of the cochlea and not within the cochlear tissues. These findings demonstrate the settlement of BMSC-derived cells within the cochlear tissues, particularly within the SL and SLB, after transplantation into the perilymphatic space of cochleae, suggesting the potential of BMSCs for migration into the SL and the SLB. These observed trends in the sites for BMSC migration indicate that the cells are suitable candidates for delivering genes in these regions, because delivery of cochlear constructive proteins may be required for the settlement of genetically manipulated cells in the regions in which encoded proteins should be expressed.

The gap junction network in the SL and the SLB has been suggested to play a crucial role in the maintenance of the endocochlear potential, which is necessary for hearing [13,14]. Our data demonstrate that some of the BMSC-derived cells that settled in the cochleae expressed Cx26, indicating the possible use of BMSC transplantation for restoration of the gap junction network in the cochlear connective tissues. The number of BMSC-derived cells expressing Cx26, however, may not be sufficient for the restoration of the gap-junction network. We should develop further strategies for increasing the number of BMSC-derived cells that settle within these regions to realize cochlear functional recovery by BMSC transplantation.

Immunohistochemical analyses in this study demonstrated no transdifferentiation of BMSCs into the neural or epithelial lineage after transplantation into the cochleae. In contrast to these findings, previous studies have demonstrated that BMSCs can differentiate into various types of cells including a neural lineage [15,16]. Naito *et al.* [17] have reported a differentiation of BMSCs into neurons after transplantation into the modiolus of chinchilla cochleae that had been damaged by aminoglycosides; however, the number of BMSC-derived cells expressing a neural marker is very limited. In this study, we identified the expression of nestin in BMSCs before and after transplantation, although the number is very limited. We therefore consider that neural induction of BMSCs and selection of neural progenitors from BMSC-derived cells before transplantation might be necessary to achieve the restoration of cochlear neurons through the transplantation of BMSCs.

Conclusion

In summary, our current findings demonstrate that BMSCs have the capability to survive in the cochlea and migrate into the cochlear tissues, which indicates possible use of BMSC transplantation as a strategy for the treatment of SNHL. Further studies are, however, necessary to realize the practical use of BMSC transplantation for the treatment of inner ears.

Acknowledgements

The authors thank Y. Nishiyama and R. Sadato for their technical assistance. This study was supported, in part, by a Grant-in-Aid for Scientific Research (B2, 16390488) from the Ministry of Education, Culture, Sports, Science and Technology of Japan, by a grant from the Takeda Science Foundation and by Higher Education Commission, Islamabad, Pakistan and Ministry of Science and Technology of Pakistan.

References

1. Tateya I, Nakagawa T, Iguchi F, Kim TS, Endo T, Yamada S, *et al.* Fate of neural stem cells grafted into injured inner ears of mice. *Neuroreport* 2003; **14**:1677–1681.
2. Izumikawa M, Minoda R, Kawamoto K, Abrashkin KA, Swiderski DL, Dolan DF, *et al.* Auditory hair cell replacement and hearing improvement by Atoh1 gene therapy in deaf mammals. *Nat Med* 2005; **11**:271–276.
3. Okano T, Nakagawa T, Endo T, Kim TS, Kita T, Tamura T, *et al.* Engraftment of embryonic stem cell-derived neurons into the cochlear modiolus. *Neuroreport* 2005; **16**:1919–1922.
4. Yagi M, Magal E, Sheng Z, Ang KA, Raphael Y. Hair cell protection from aminoglycoside ototoxicity by adenovirus-mediated overexpression of glial cell line-derived neurotrophic factor. *Hum Gene Ther* 1999; **10**: 813–823.
5. Chen X, Frisina RD, Bowers WJ, Frisina DR, Federoff HJ. HSV amplicon-mediated neurotrophin-3 expression protects murine spiral ganglion neurons from cisplatin-induced damage. *Mol Ther* 2001; **3**:958–963.
6. Hakuba N, Watabe K, Hyodo J, Ohashi T, Eto Y, Taniguchi M, *et al.* Adenovirus-mediated overexpression of a gene prevents hearing loss and progressive inner hair cell loss after transient cochlear ischemia in gerbils. *Gene Ther* 2003; **10**:426–433.
7. Okano T, Nakagawa T, Kita T, Endo T, Ito J. Cell-gene delivery of brain-derived neurotrophic factor to the mouse inner ear. *Mol Ther* 2006; **14**: 866–871.
8. Nagaya N, Kangawa K, Itoh T, Iwase T, Murakami S, Miyahara Y, *et al.* Transplantation of mesenchymal stem cells improves cardiac function in a rat model of dilated cardiomyopathy. *Circulation* 2005; **112**:1128–1135.
9. Oshima K, Shimamura M, Mizuno S, Tamai K, Doi K, Morishita R, *et al.* Intrathecal injection of HVJ-E containing HGF gene to cerebrospinal fluid can prevent and ameliorate hearing impairment in rats. *FASEB J* 2004; **18**:212–214.
10. Iwai K, Nakagawa T, Endo T, Matsuoka Y, Kita T, Kim TS, *et al.* Cochlear protection by local IGF-1 application using biodegradable hydrogel. *Laryngoscope* 2006; **116**:526–533.
11. Picciotti PM, Fetoni AR, Paludetti G, Wolf FI, Torsello A, Troiani D, *et al.* Vascular endothelial growth factor (VEGF) expression in noise-induced hearing loss. *Hear Res* 2006; **214**:76–83.
12. Okabe M, Ikawa M, Kominami K, Nakanishi T, Nishimune Y. 'Green mice' as a source of ubiquitous green cells. *FEBS Lett* 1997; **407**:313–319.
13. Xia A, Kikuchi T, Hozawa K, Katori Y, Takasaka T. Expression of connexin 26 and Na, K-ATPase in the developing mouse cochlear lateral wall: functional implications. *Brain Res* 1999; **846**:106–111.
14. Hirose K, Liberman MC. Lateral wall histopathology and endocochlear potential in the noise-damaged mouse cochlea. *J Assoc Res Otolaryngol* 2003; **4**:339–352.
15. Dezawa M, Hoshino M, Ide C. Treatment of neurodegenerative diseases using adult bone marrow stromal cell-derived neurons. *Expert Opin Biol Ther* 2005; **5**:427–435.
16. Lu J, Moochhala S, Moore XL, Ng KC, Tan MH, Lee LK, *et al.* Adult bone marrow cells differentiate into neural phenotypes and improve functional recovery in rats following traumatic brain injury. *Neurosci Lett* 2006; **398**:12–17.
17. Naito Y, Nakamura T, Nakagawa T, Iguchi F, Endo T, Fujino K, *et al.* Transplantation of bone marrow stromal cells into the cochlea of chinchillas. *Neuroreport* 2004; **15**:1–4.

Equilibrium Res Vol. 64(2) 100～105, 2005

原　著

微細刺激によるクプラの偏移の観察

大塚　康司[1]・鈴木　衛[2]・古屋　正由[3]
小川　恭生[2]・萩原　晃[2]・竹之内　剛[4]

Displacement of the Cupula Due to Endolymphatic Pressure Change

Koji Otsuka[1], Mamoru Suzuki[2], Masayoshi Furuya[3],
Yasuo Ogawa[2], Akira Hagiwara[2], Tsuyoshi Takenouchi[4]

[1] *Department of Otolaryngology, Kosei Chuo Hospital*
[2] *Department of Otolaryngology, Tokyo Medical University*
[3] *Department of Otolaryngology, Toda Chuo Hospital*
[4] *Department of Otolaryngology, Tokyo Medical University, Hatioji Medical Center*

Whole membranous labyrinths of the bull frogs were used in order to replicate the human vestibule. The posterior semicircular canals (PSC) were exposed leaving the remaining membranous labyrinth encapsulated in the otic capsule. The membranous labyrinth was cut by 0.5 mm at the crus commune to create a tiny opening. The cupula was visualized by gently injecting India ink of the opening. The motion of the cupula was analyzed during compression of the canal wall by a needle. The motion appeared to be that of a "diaphragma" when the compression was weak. The motion appeared to be that of a "swing door" with the base of the cupula hinged on the crista when the compression was strong.

A small piece of otoconia removed from the sacculus of the other ear was introduced through this opening into the canal lumen. The position of the preparation was controlled so that the otoconia were attached onto the cupular surface. This was regarded as a cupulolithiasis model. We performed the same experiments on the cupulolithiasis models and results were almost same, except that the motion of the cupula of cupulolithiasis models was shorter than those of the normal models. It was inferred that the motion of the cupula of cupulolithiasis models was suppressed by the weight of the otoconia.

It was observed that the india ink traversed the cupula during the compression and even the otoconia traversed the cupula. Therefore, it was inferred that the adhesion of the cupula and the ampula wall is not strong, thus protecting the cupula from detaching from the crista.

Key words: cupula, diaphragma, swing door, cupulolithiasis

[1] 厚生中央病院耳鼻咽喉科　[2] 東京医科大学耳鼻咽喉科　[3] 戸田中央病院耳鼻咽喉科
[4] 東京医科大学八王子医療センター耳鼻咽喉科

はじめに

クプラは，その形状，運動様式などからきわめて興味深い研究対象である。しかしながら，それ自体がきわめて脆弱であり生体内で観察困難なことから，その生理学的機能については未だ不明な点が多い。近年，良性発作性頭位めまい症（BPPV）の病態が明らかにされてきており，典型例は半規管結石症とされる。また半規管結石症という病態がクプラ結石症に変化したり，その逆のこともある。これらにはクプラと耳石との接着性が関与しており，その意味でもクプラの物理，化学的特性を研究する意義は大きいと考えられる。

両生類，とくにウシガエルの半規管は膜迷路が強靭で，しかも形態学的，生理学的に哺乳類のそれと酷似していることからこの面の研究に適している。今回，生理的に近い状態で墨汁を半規管内に注入し，クプラを染色，観察することを試みた。膜迷路への微細な圧迫刺激によりクプラを偏移させ，その移動距離を計測した。それにより内リンパが移動したときクプラがどのように偏移するかが観察できた。またクプラに耳石が付着したクプラ結石症のモデルにおいても同様の実験を行った。さらにクプラと膨大部壁との接着状態についても検討したので報告する。

対象と方法

実験１　微細刺激による正常クプラの偏移

ウシガエル（Rana catesbeiana）を用いた。Harada[1] らが報告した方法で口蓋側より骨迷路を一塊として摘出し，後半規管の膜迷路を露出した。実体顕微鏡下に総脚部の膜迷路に微小切開を加え，墨汁を注入した。墨汁が膨大部に到達するとクプラ表面が墨汁で染まり，表面の輪郭が観察できた。膨大部と半規管の移行部の半規管壁をマイクロマニピュレータに装着した注射針にて定量的に圧迫することによりリンパの移動を起こし，クプラを偏移させた（図１）。その際，針を進めて，クプラの動きがわずかでも顕微鏡下で確認できたところを起点とし，そこからさらに10，20，30，40 μm と針を進めた。クプラ側面において，基部（膨大部稜側）をＡ点，クプラの中間部をＢ点，クプラの先端部をＣ点とし，それぞれの移動距離を計測した（図２）。標本作製に要する時間は約30分である。なお実験はすべて室温（15～20°C）下カエル用リンゲル液内（NaCl 6.46 g/l, KCl 0.19 g/l, $CaCl_2$ 0.20 g/l, $NaHCO_3$ 0.20 g/l）で行った。

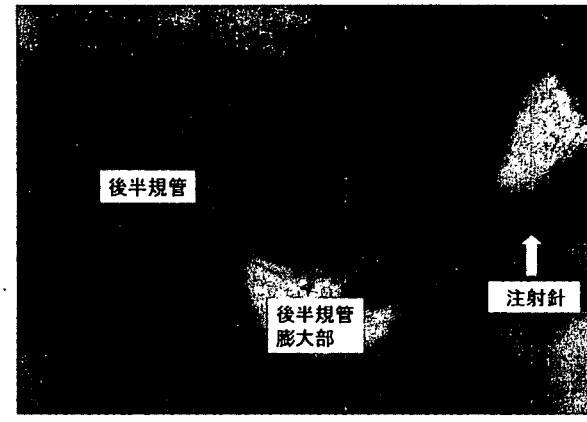

図１　微細刺激時の実体顕微鏡写真
墨汁を注入してクプラを透亮像で観察できるようにした後，半規管の一部を注射針にて定量的に圧迫することによりリンパの移動を起こし，クプラを偏移させた。

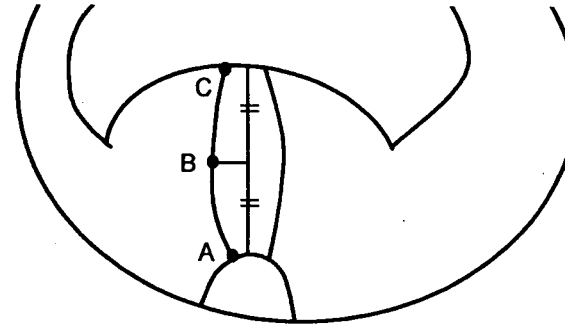

図２　クプラの計測点
クプラ側面において，基部（膨大部稜側）をＡ点，クプラの中間部をＢ点，クプラの先端部をＣ点とし，それぞれの移動距離を計測した。計測は，記録した画像上で行い，圧迫前のＡ，Ｂ，Ｃ点をプロットし，次に圧迫後の各点をプロットして，それらを重ね合わせた像からクプラの移動距離を測定した。

計測は，デジタルビデオ記録した画像上で行った。圧迫前のＡ，Ｂ，Ｃ点をコンピューター画面上にプロットし，次に圧迫後の各点をプロットして，それらを重ね合わせた像からクプラの移動距離を測定した。移動距離はクプラ側面全長に対する百分率で表した。４標本を使用した。

実験２　クプラ結石症におけるクプラの偏移

実験１と同様に骨迷路を一塊として摘出した。以前に報告した方法[2] で反対側の球形嚢耳石の小

塊を総脚の切開部より挿入し，それを膨大部に移動させクプラに付着させた。これをクプラ結石症のモデルとし，同様の方法でクプラの偏移を測定した。3標本を使用した。

実験3　クプラと膨大部壁との接着性

クプラと膨大部壁との接着状態を検討するために圧迫刺激下に墨汁がクプラを越えて移動するか否かを観察した。

また，半規管結石症モデルにおける結石の移動についても検討した。7標本を使用した。

結　　果

実験1　微細刺激による正常クプラの偏移

圧迫量と各測定点におけるクプラの移動距離を表1，図3に示す。圧迫 10 μm ではB点のみにおいて平均5.6±1.6%の移動を示し，20 μm のときにはやはりB点のみにおいて平均6.8±1.3%の移動を示した。30 μm ではB点で平均6.8±1.6%，C点で平均11.4±2.2%移動し，40 μm ではB点で平均7.8±1.7%，C点で平均12.1±1.8%移動した。つまり迷路への圧迫刺激が弱いときにはB点のみが動き diaphragma 様運動（両端が固定された隔膜が圧力を受けて弧状になる動き）が観察され，圧迫刺激が強くなるとC点の方がB点より大きく動き，膨大部稜を蝶番とする swing door 様運動（ワイパーのような片端が固定されてそこを基点とする動き）が観察された。また持続的な圧迫刺激を与えている間，クプラは少なくとも10分間偏移したままの位置に留まっているのが観察された。その後，しばらくそのままの位置に留まっている標本もあれば，徐々に元の位置に戻る標本もあった。

表1　正常クプラ偏移の平均値
移動距離はクプラ側面全長に対する百分率で表した。圧迫距離が短いときにはB点のみが動き，圧迫距離が長くなるとC点の方がB点より大きく動いた。

測定点 / 圧迫距離	A点	B点	C点
10 μm	0	5.6±1.6	0
20 μm	0	6.8±1.3	0
30 μm	0	6.8±1.3	11.4±2.2
40 μm	0	7.8±1.7	12.1±1.8

単位：%

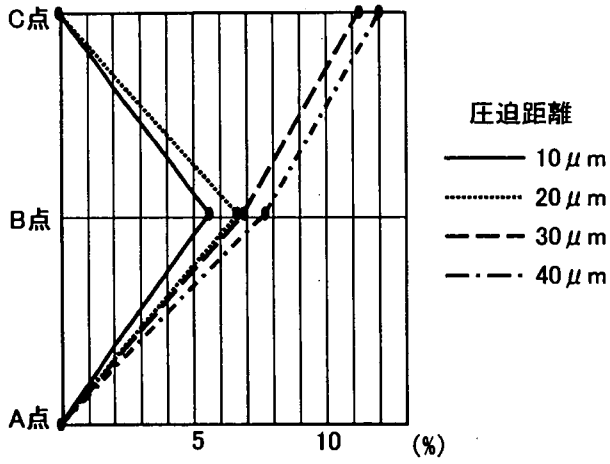

図3　正常クプラ偏移の平均値のグラフ
各点でのクプラの偏移を示す。

実験2　クプラ結石症におけるクプラの偏移

図4はクプラに耳石を付着させ，さらに墨汁を半規管内に注入した状態である。

圧迫距離と各測定点におけるクプラの移動距離を表2，図5に示す。圧迫が 10 μm ではB点のみにおいて平均5.2±0.8%の移動を示し，20 μm のときにはやはりB点のみにおいて平均6.7±1.8%移動した。30 μm ではB点で平均6.7±1.8%，C点で平均9.0±2.6%移動し，40 μm ではB点で平均7.7±2.1%，C点で平均11.8±1.8%移動した。圧迫量が小のときは diaphragma 様運動が，圧迫量が大のときは swing door 様運動が観察され，クプラの運動様式は正常時と同様であった。またクプラ結石症の状態ではクプラの移動距離が正常のクプラよりやや短い傾向はあったが，有意差はなかった。

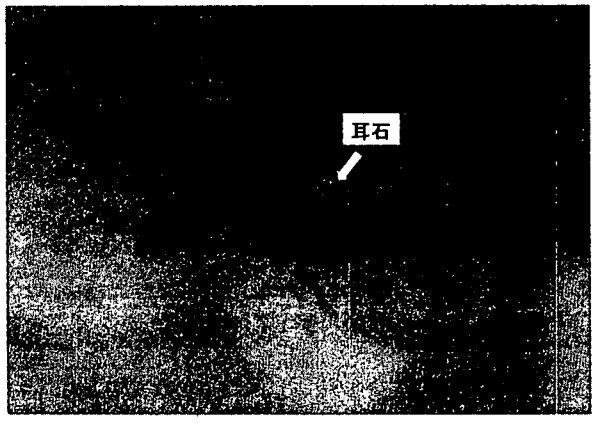

図4　クプラ結石症モデルの実体顕微鏡写真

表2　クプラ結石症におけるクプラ偏移の平均値
移動距離はクプラ側面全長に対する百分率で表した。圧迫距離が短いときにはB点のみが動き，圧迫距離が長くなるとC点の方がB点より大きく動くことは正常時と同様であったが移動距離は短い傾向があった。

測定点 / 圧迫距離	A点	B点	C点
10 μm	0	5.2±0.8	0
20 μm	0	6.7±1.8	0
30 μm	0	6.7±1.8	9.0±2.6
40 μm	0	7.7±2.1	11.8±1.8

単位：%

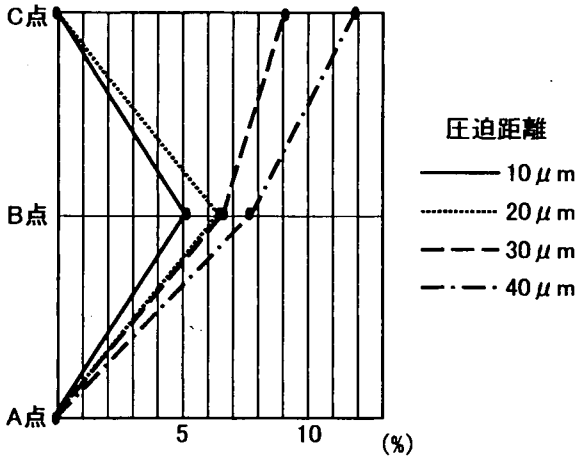

図5　クプラ結石症におけるクプラ偏移の平均値のグラフ
各点でのクプラの偏移を示す。

実験3　クプラと膨大部壁との接着性

墨汁を半規管内に注入していくと，クプラに到達した墨汁はその表面で留まっていた。しかし，微細圧迫刺激を加えると墨汁はクプラの上端部より少量ずつクプラの反対側に移動した。圧迫量をさらに上げていくと墨汁がクプラ中央部の溝状部から膨大部壁の間を通り抜けるのが観察された（図6）。

半規管結石症モデルを作製し耳石を移動させると，クプラと膨大部壁との間を耳石が通り抜けて移動する現象がみられた（図7）。

考　察

クプラの運動様式については，従来より意見が分かれていた。1931年にSteinhausen[3]が魚類の半規管に墨汁を注入してクプラを明視し，運動様式を観察した。彼は人工的な内リンパ流動によりクプラが基部を蝶番とするswing-door様運動をするのを観察した。Dohlman[4]も同様の実験を行いクプラのswing-door様運動を観察したが，生理的動作による内リンパ流動ではこのような大きな動きではなくきわめて小さな動きであろうと推

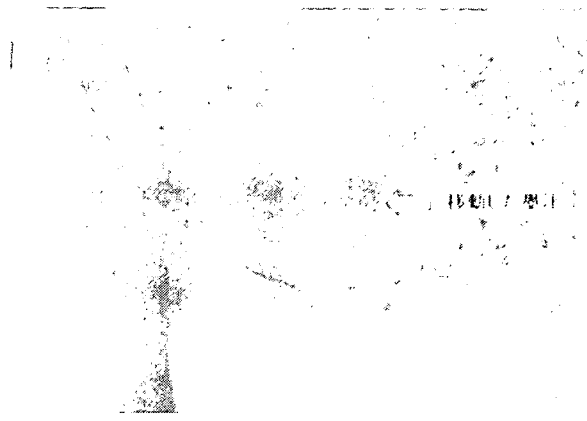

図6　クプラを通り抜けて移動する墨汁
墨汁を半規管内に注入していくと，到達した墨汁はクプラ表面で留まっていたが，圧迫刺激を繰り返し加えると墨汁はクプラの上端部より反対側に移動した。

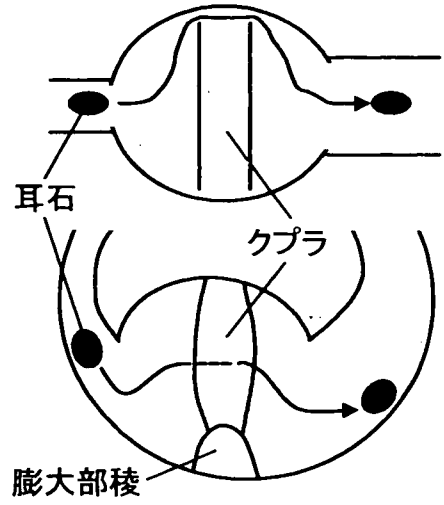

図7　クプラ側面と膨大部壁を通り抜ける耳石の模式図
半規管結石症モデルを作製し耳石を移動させると，クプラ側面と膨大部壁との間を耳石が通り抜けて移動する現象がみられた。
上：膨大部頂部からの図
下：膨大部側面からの図

測している。一方, McLaren ら[5] はマイクロピペットにてクプラに直接マーキングを行ったのち，微量のリンパ流動下に diaphragma 様運動を観察した。ただ，この方法ではクプラや膨大部壁に対し直接的な機械的損傷が加わる可能性がある。Hillman ら[6] は，微量の内リンパ流動ではクプラ下部が動き，刺激量の増大に伴いクプラ中央部が最大に動いて diaphragma 様運動となり，さらに強い力が加わると swing-door 様運動を始めると報告した。Oman ら[7] は，クプラと膨大部壁との接着状態は強くはないため，強大な力が加わるとクプラと壁との接着が解離して swing-door 様運動が起こると述べている。

今回の実験では，できるだけクプラやその周辺に影響が及ばないことを狙って総脚に作製した小孔を通して墨汁を注入しクプラを明視できるようにした。その結果は Hillman ら[6] の報告とほぼ同様であった。平常の場合クプラは膨大部壁との接着が保たれ diaphragma 様運動をしているが，過大なリンパ流動下では接着が疎となり，swing-door 様運動となる。すなわち，クプラの運動はクプラと膨大部との接着状態により大きく変わってくると考えられた。またウシガエル後半規管のクプラ側面の長径を 400 μm とする[8] と diaphragma 様運動ではクプラの中央部が約 20 μm, swing-door 様運動ではクプラの先端部が約 40 μm 移動すると換算できた。クプラの中央部が 20 μm 動いた際に感覚毛側でどの程度クプラが偏移するかは明らかにできなかった。おそらく数 μm かそれ以下の偏移と思われるが，クプラや周囲構造が変化した所見はなかったので，少なくとも生理的な刺激量の範囲と想像される。なお，Hillman ら[6] の報告では，微量の圧力では B 点よりやや下部に偏移のピークがあり，少し圧力が加わると B 点付近が偏移のピークになるとしている。つまり圧力によっても偏移のピークを示す場所が変わると考えられる。今回は便宜上，中央部を測定点として計測した。

鈴木ら[9][10] はクプラの一部を微細ガラス管で直接圧迫して，その活動電位を計測し，クプラの基部を圧迫した方が上部を圧迫するより刺激効果が大であったと報告した。このことからも，diaphragma 様運動により感覚上皮は有効に刺激されていると考えられた。

クプラ結石症の場合も基本的にはクプラの動きは同様であったが，移動距離は短い傾向があった。これは，クプラに付着した耳石の重量のためにクプラの動きが制限されたと推測できる。BPPV では温度眼振反応[11][12] や回転刺激時の VOR の利得[13] が低下するとの報告があり，クプラ結石症の関与が推測された。現在，半規管結石症やクプラ結石症モデルに振子様回転刺激を加え半規管活動性の変化を検討中である。

次にクプラと膨大部壁との接着状態を墨汁の移動を指標に観察した。刺激のない状態では墨汁はクプラの片側に留まっているが，刺激を繰り返すとクプラを越え反対側に移動するのが観察された。また耳石はクプラの周辺を越えて移動することがあり，これが BPPV の病態の変化に関係している可能性が示唆された。いかなる場合にこのような通り抜けが起こるかは明らかでないが，耳石の量や粘度が関係していると考えられる。一定重量以上の耳石塊がクプラの端，つまり膨大部壁近傍に到達すると重量の作用で反対側に抜けていくようである。

以上より，クプラは平常では半規管膨大部壁に密着してリンパを遮断しているが，圧迫刺激を繰り返すと一部，壁から解離してリンパが移動する。また耳石塊がクプラと壁の間を通り抜けることがある。クプラはその主成分がシアロ糖蛋白質[14] で水分に富んでおり脆弱であるが，クプラと壁との接着状態も強くはないと考えられる。圧迫量が過大になると，墨汁はクプラ中央の溝状部から膨大部壁の間を通り抜けるのが観察された。これは過大な刺激が加わったとき，リンパ流を逃がすことによりクプラが膨大部稜から遊離するのを防ぐ一種の防御機構と推測された。

ま と め

1，迷路への圧迫刺激が弱いときには，クプラは diaphragma 様運動を示した。

2，迷路への圧迫刺激が強いときには，膨大部稜を蝶番とする swing-door 様運動が観察された。

3，正常の状態とクプラ結石症の状態では運動様式や移動距離に有意差はなかった。

4，迷路への持続的な圧迫刺激を与えている間は，クプラは偏移したままの位置に留まっているのが観察された。

5，半規管結石症モデルにおいて結石がクプラ

を越えて移動するのが観察された。

なお，本論文の要旨は，第61回日本めまい平衡医学会（2002年，富山市）において発表した。

文　献

1）Harada Y, Musso E: Study of the action potential in the isolated posterior ampullar receptor. Acta Otolaryngol 72: 274–280, 1971

2）Otsuka K, Suzuki M, Furuya M: Model experiment of benign paroxysmal positional vertigo mechanism using the whole membranous labyrinth. Acta Otolaryngol 123: 515–518, 2003

3）Steinhausen W: Über den Nachweis der Bewegung der Cupula in der intakten Bogengangsampulle des Labyrinthes bei der natürlichen rotatorischen and calorischen Reizung. Pflügers Arch Gesamte Physiol Menschen Tiere 228: 322–328, 1931

4）Dohlman GF: The attachment of the cupulae, otolith and tectorial membranes to the sensory cell areas. Acta Otolaryngol 71: 89–105, 1971

5）McLaren JW, Hillman DE: Configuration of the cupula during endolymph pressure changes. Soc Neuroscience Abs 2: 1060, 1976

6）Hillman DE, McLaren JW: Displacement configuration of semicircular canal cupulae. Neuroscience 4: 1989–2000, 1979

7）Oman CM, Frishkoph LS, Goldstein MH Jr: Cupula motion in the semicircular canal of the skate, Raja erinacea. An experimental investigation. Acta Otolaryngol 87: 528–538, 1979

8）鈴木　衞，原田康夫，有木　健，他：半規管機能モデルの研究．耳鼻臨床 77: 1993–2001, 1984

9）鈴木　衞，原田康夫：半規管クプラの実験的研究—クプラの直接刺激法について—．耳鼻臨床 77: 2547–2552, 1984

10）鈴木　衞，原田康夫：半規管クプラの実験的研究—とくにクプラの mapping について—．耳鼻臨床 78: 103–108, 1985

11）Baloh RW, Honrubia V, Jacobson K: Benign positional vertigo: clinical and oculographic features in 240 cases. Neurology 37: 371–378, 1987

12）Korres SG, Balatsouras DG, Ferekidis E: Electoronystagmographic findings in benign paroxysmal positional vertigo. Ann Otol Rhinol Laryngol 113: 313–318, 2004

13）Sekine K, Imai T, Nakamae K: Dynamics of the vestibulo-ocular reflex in patients with the horizontal semicircular canal variant of benign paroxysmal positional vertigo. Acta Otolaryngol 124: 587–594, 2004

14）佐藤修治：クプラ，クプラ下腔に関する形態学的，電気生理学的および組織化学的研究．耳鼻臨床 81: 433–452, 1988

原稿到着：平成17年1月14日

別刷請求先：大塚康司
〒153–0073 東京都目黒区三田1–11–7
厚生中央病院耳鼻咽喉科
E-mail: otsukaent@aol.com

ORL

ORL 2005;67:266–271
DOI: 10.1159/000089406

Published online: December 15, 2005

Contribution of Endolymphatic Fluid Shift to Caloric Response in Plugged Semicircular Canals

Tsuyoshi Takenouchi Mamoru Suzuki Masayoshi Furuya Koji Otsuka
Yasuo Ogawa

Department of Otorhinolaryngology, Tokyo Medical University, Tokyo, Japan

Key Words

Caloric response · Thermoconvective flow · Fluid shift · Canal plugging · Posterior semicircular canal · Compound action potentials

Abstract

The purpose of this study was to clarify the role of endolymphatic fluid shift in caloric response, using frog posterior semicircular canals (PSCs). PSCs were sutured using 10-0 nylon thread and were used as a model of canal plugging. Compound action potentials (CAPs) of the PSC nerve evoked by a cooling stimulus were recorded. The CAPs after suturing the PSCs were found to be greater than those before suturing. This indicates that the fluid shift effect increases after canal suturing. Additionally, we present a clinical case in which caloric nystagmus was observed after lateral canal plugging. In this case MRI revealed the fluid space from the plugged portion toward the ampulla to be intact. There was another case with lateral canal plugging that showed the same findings on MRI. The above findings support the hypothesis that fluid shift is responsible for the caloric response without the convective flow of endolymph in the plugged canal.

Introduction

The mechanism of the caloric response is controversial. Thermoconvective flow is considered to be the most plausible mechanism involved. However, there have been reports that the caloric nystagmus is observed even under microgravity and in monkeys with plugged canals [1, 2]. The endolymphatic fluid shift effect [3] and the direct thermal effect on the vestibular receptor [4] have also been proposed as possible mechanisms.

The purpose of this study was to quantify the contribution of the contraction of the endolymph to the caloric response, using sutured posterior semicircular canals in the frog.

Materials and Methods

Experiment Using Isolated Labyrinths

This experiment was conducted to quantify the effect of canal plugging on the endolymphatic fluid shift using the sutured posterior semicircular canal (PSC) as a plugging model. Six bullfrogs *(Rana catesbeiana)* weighing 80–150 g were used. The frogs were heavily anesthetized with diethyl ether. After decapitation, the entire bony labyrinth was removed and placed in frog Ringer's solution. The membranous labyrinth of the PSC was exposed, leaving the bony labyrinth intact. The preparation was placed in a dish, and frog Ringer's solution was filled in up to the level of the upper

KARGER

Fax +41 61 306 12 34
E-Mail karger@karger.ch
www.karger.com

0301–1569/05/0675–0266$22.00/0

Accessible online at:
www.karger.com/orl

Tsuyoshi Takenouchi, MD
Department of Otorhinolaryngology, Tokyo Medical University
6-7-1, Nishishinjuku, Shinjuku-ku
Tokyo 160-0023 (Japan)
Tel. +81 3 3342 6111, Fax +81 3 3346 9275, E-Mail tandc@ra3.so-net.ne.jp

surface of the PSC. The inferior vestibular nerve was sucked into a glass suction electrode to record compound action potentials (CAPs). All nerve branches were cut off except for the PSC ampullary nerve.

A copper thermal probe with a tip diameter of 1 mm was dipped in liquid nitrogen for 10 s and used as a cooling stimulus. The probe was placed approximately 1 mm away from the PSC surface at the midpoint of the canal (fig. 1, 2). A thermocouple was placed 1 mm away from the thermal probe tip to monitor the temperature change. The duration of the thermal stimulus was 20 s. The canal was sutured with 10-0 nylon threads at the canal end near the common crus. The PSCs were placed in the horizontal plane to eliminate the thermoconvective flow of the endolymph. The CAPs of the PSC ampullary nerves resulting from the thermal stimuli were recorded before and after canal suturing. All experiments were carried out in accordance with the rules of the ethics committee of Tokyo Medical University.

Clinical Observations

A 61-year-old female with intractable lateral canal benign paroxysmal positional vertigo (BPPV) underwent a canal plugging operation. The MRI findings and postoperative caloric test results were analyzed. Another case was a 64-year-old female with intractable lateral canal BPPV that underwent canal plugging. The MRI findings were studied.

Results

Experiment Using Isolated Labyrinths

Temperature Change Monitored by a Thermocouple. The time course of the temperature measured by the thermocouple at the PSC surface is presented in figure 3. The temperature measured prior to the thermal stimulus was 22.1°C. When the PSC was cooled, the temperature dropped by 3.9°C in 8 s and gradually increased afterwards.

CAP of PSC before and after Thermal Stimulation. Examples of PSC CAP histograms before and after canal suturing are presented in figure 4. The CAPs were greater after canal suturing in all preparations. The duration and maximum spike counts before suturing were 23.3 ± 2.67 s and 165.0 ± 33.0 spikes/s, respectively. After suturing, the duration was 28.2 ± 3.12 s and the maximum spike count was 197.4 ± 24.8 spikes/s. The suturing of the PSC increased both the duration and the maximum spike count by approximately 20 and 17%, respectively.

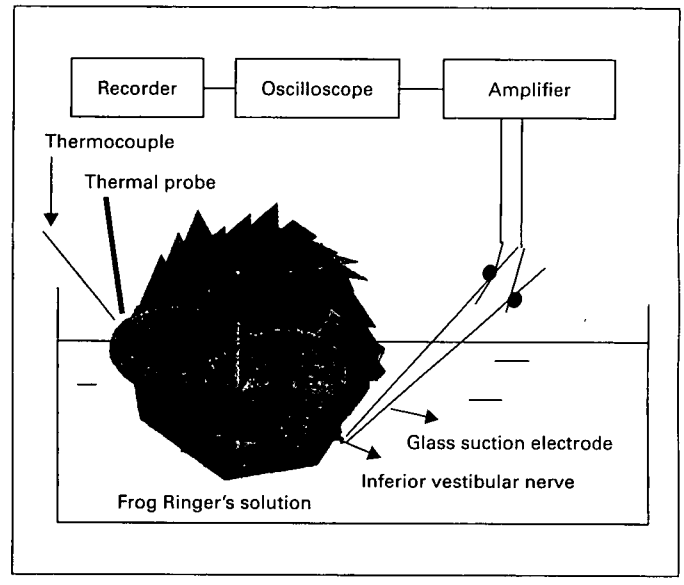

Fig. 1. Schematic diagram of the experimental setting.

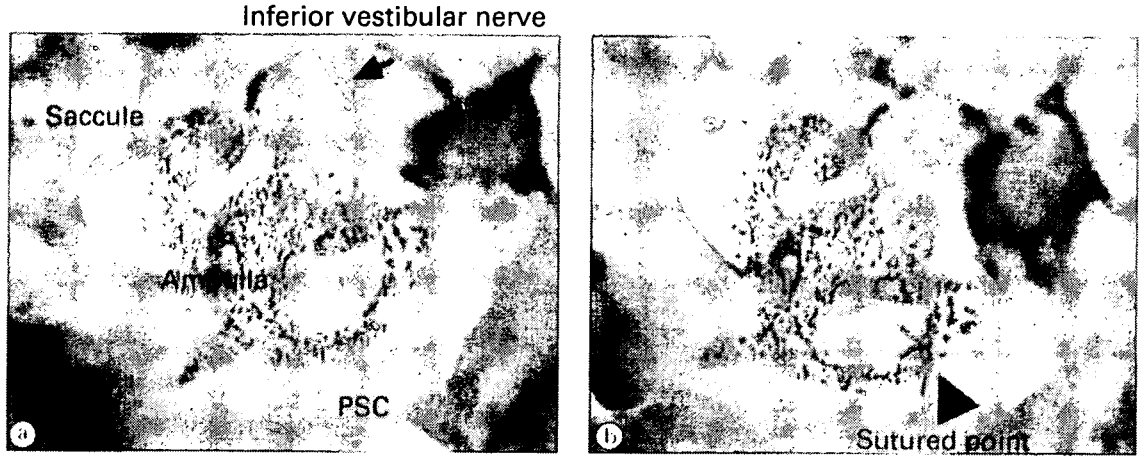

Fig. 2. Pictures of isolated labyrinths taken under the dissecting microscope. **a** Intact canal. **b** Sutured canal.

Clinical Observation

The first case was a 61-year-old female who had suffered from positional vertigo for 8 years. The equilibrium test results suggested BPPV with a lateral canalolithiasis. She underwent right lateral canal plugging on 21 June 2001. Figure 5 shows MRI images taken 1 year after the operation. The fluid space of the right lateral canal from the plugged portion to the canal end disappeared completely (indicated by the arrow in fig. 5). However, the fluid space toward the ampulla appeared intact. Caloric stimuli to the operated (right) ear using cold water induced weak but distinct left beating horizontal nystagmus. The duration and beats of the nystagmus were 48 s and 26 beats, respectively. The direction of this nystagmus did not change in the prone position. The caloric nystagmus in the left ear was normal, 146 s in duration and 196 beats. Figure 6 is an ENG recording of the left beating horizontal nystagmus of the right ear. The other case was a 64-year-old female with lateral canalolithiasis that underwent lateral canal plugging on 20 April 1999. The MRI taken 4 years after the plugging also revealed non-fluid space toward the canal end and fluid space toward the ampullary side as was shown in the first case.

Discussion

Since Bárány's report (1906), the caloric response had been attributed to the thermoconvective flow of the endolymph. After the nystagmus was observed under microgravity and in a canal-plugged monkey, the endolymphatic fluid shift has been proposed to be another relevant

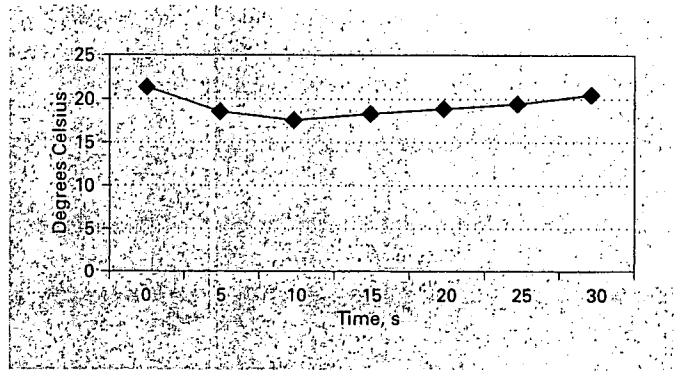

Fig. 3. Time course of temperature change by cooling stimulus recorded at PSC surface.

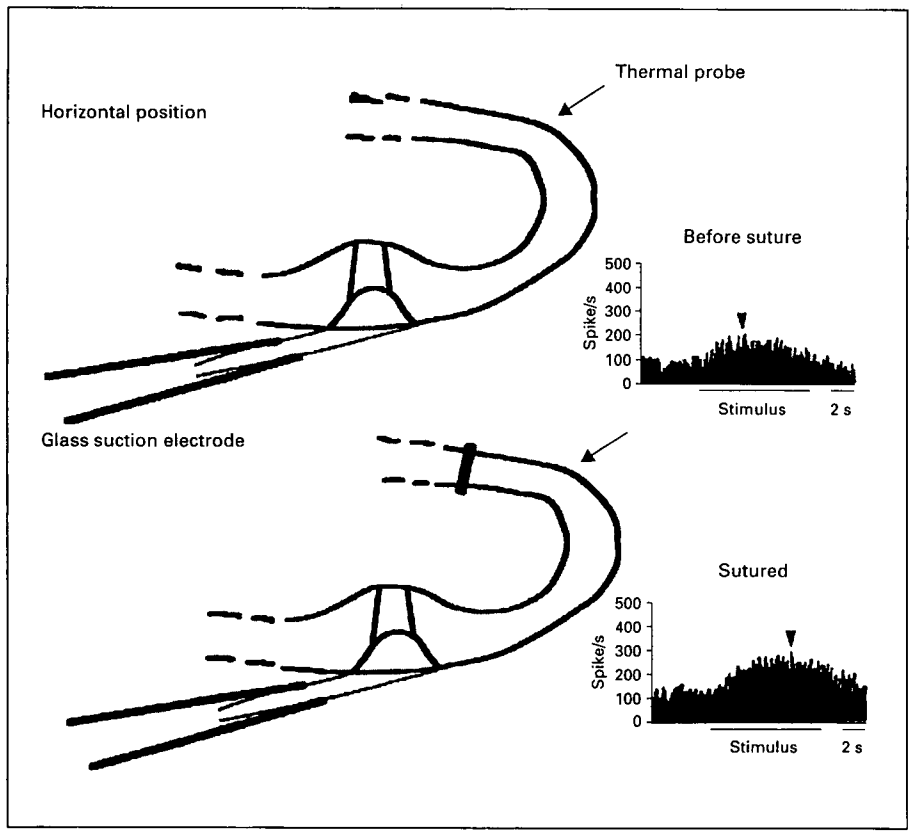

Fig. 4. Example of PSC CAP histograms before and after canal suturing. Small arrows indicate maximum spike counts of CAP. This diagram emphasizes PSCs. CAP is greater after canal suturing.

mechanism. However, the effect of the fluid shift and canal plugging on caloric response has not yet been quantified. The isolated frog labyrinth is suitable for this study because its physiological activity can be maintained in frog Ringer's solution.

To examine the effect of canal plugging, we compared the CAPs of the intact and sutured PSCs. The duration and maximum spike counts of the PSC were found to be greater after canal suturing. This increase is possibly due to an increase in the fluid shift effect, which leads to contraction of endolymph in the sutured canal. Figure 7 presents a scheme of the mechanism of the increased fluid shift effect. Cooling results in the localized increase in endolymphatic density and reduction of endolymphatic volume. This produces endolymphatic shift. The amount of endolymphatic shift is determined by the change of its density. There is no difference in the total amount of shift between the intact canal and the sutured canal (fig. 7, d1 + d2 = d3 + d4). In an intact canal, there is no restriction in endolymphatic fluidity. An equal amount of endolymphatic shift occurs on both ampullary side and distal side (fig. 7, d1 = d2). However, after plugging, the endolymphatic shift is inhibited on the plugged side (fig. 7, d3 > d4). Thus, more fluid shift occurs on the ampullary side (fig. 7, d1 < d3), yielding greater ampullofugal flow and greater PSC discharge. This increased fluid shift probably plays a significant role in determining the caloric response after plugging in the monkey [5].

In the clinical setting, caloric testing is performed in a supine position with slight head flexion. This is the optimum position to maximize caloric nystagmus due to the thermoconvective effect. No nystagmus is observed in the

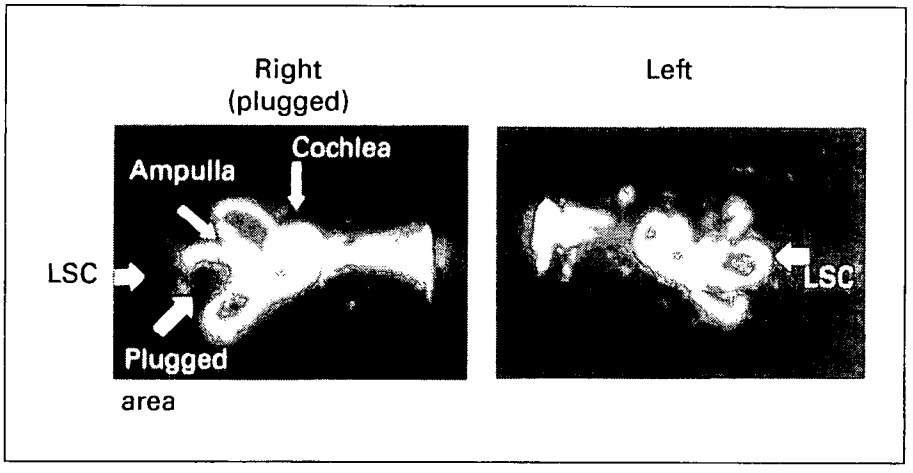

Fig. 5. MRI image taken 1 year after the operation. The fluid space from the plugged portion to the canal end completely disappeared but the fluid space toward the ampulla is still intact. LSC = Lateral semicircular canal.

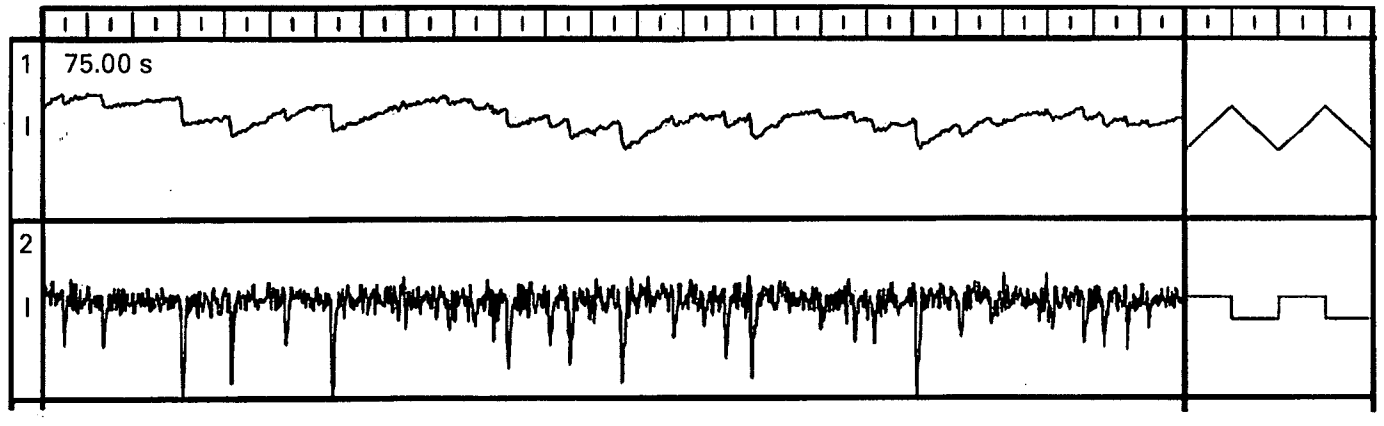

Fig. 6. ENG recording of the right ear canal after plugging. Left beating horizontal nystagmus was recorded. The nystagmus was weak but distinctive.

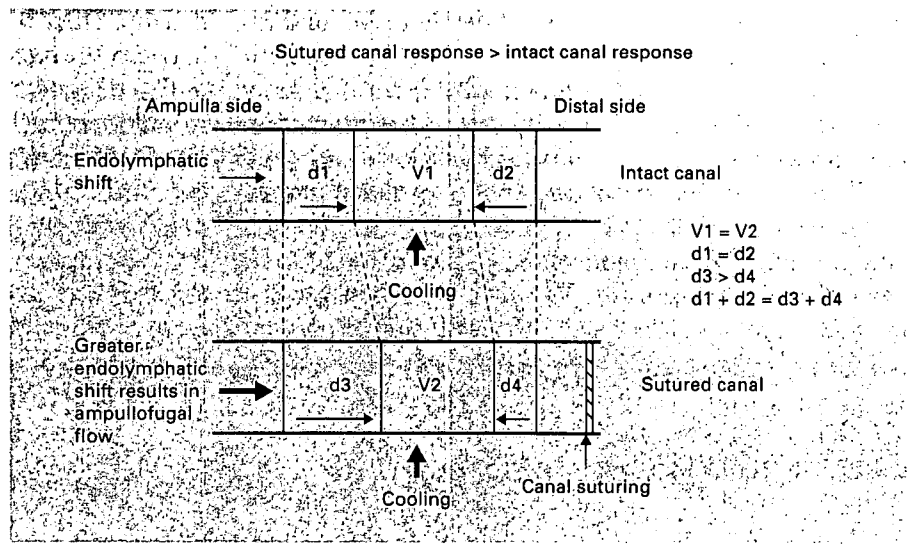

Fig. 7. Mechanism of increased response in the sutured canal. The figure shows a longitudinal cross section model of semicircular canals. V = Local endolymph volume after cool stimulus was given; d = amount of endolymphatic fluid shift; V1 = volume in an intact canal after cooling; V2 = volume in a sutured canal after cooling; d1 = amount of endolymphatic fluid shift of ampullary side in an intact canal; d2 = amount of endolymphatic fluid shift of the distal side in an intact canal; d3 = amount of endolymphatic fluid shift of ampullary side in a sutured canal; d4 = amount of endolymphatic fluid shift of the distal side in a sutured canal. The upper graph indicates an intact canal and the lower one a sutured canal. When a part of the canal is cooled, the localized endolymph increases in density and reduces its volume. This results in endolymphatic shift. In an intact canal, the fluid shifts by d1 and d2 from both sides, thus local endolymphatic volume diminishes to V1. When the canal is sutured, the total amount of local endolymphatic shift is the same as that of an intact canal. The local endolymphatic volume reduces to V2 (V1 = V2, d1 + d2 = d3 + d4), but the suture inhibits fluid shift, resulting in a smaller fluid shift on the distal side. Instead, there is a greater fluid shift on the ampullary side (d3 > d4), which results in greater ampullofugal flow.

sitting position with the lateral canal in the horizontal plane. After lateral canal plugging, the only factor contributing to caloric nystagmus is the fluid shift effect, even in the supine position. However, in our clinical case with lateral canal plugging, the cooling stimulus induced a distinct nystagmus. The enhanced fluid shift effect as observed in our experiment using frog labyrinths possibly contributed to this nystagmus. The nystagmus direction was toward the left, indicating that the cooling stimulus reduces the endolymphatic volume, thus leading to the ampullofugal fluid shift on the ampullary side. Under normal conditions, the nystagmus reverses its direction in the prone position since the thermoconvective flow exerts a fluid flow in a direction opposite to that in the supine position. In our clinical case, the direction of nystagmus did not change in the prone position. This also supports the hypothesis that only the fluid shift effect works without the thermoconvective effect.

MRI images of our cases showed that the fluid space of the lateral canal toward the ampullary side remained intact even 1 year and 4 years after canal plugging. This is probably because the endolymphatic homeostasis is maintained in the nonsensory epithelia including the dark cells and permeable sections of the inner ear membrane [6, 7]. Suzuki [8] also reported that the sensory epithelia remained intact after canal plugging in the monkey. The finding that only the ampulla secretes K-rich fluid in the semicircular canal [9] supports the physiological viability of the canal after plugging.

The thermoconvective flow of the endolymph still plays a major role in determining the caloric response. Our study showed that the fluid shift effect is at least a part of the mechanism of the caloric response.

Acknowledgment

This study was supported by Health and Labor Science Research Grants in Japan (Research on Measures for Intractable Diseases).

References

1 von Baumgarten R, Benson A, Brand U, Bandt T, Bruzek W, Dichgans J, Probst T, Scherer H, Vieville T, Vogel H, Wetzig J: Effects of rectilinear acceleration and optokinetic and caloric stimulation in space. Science 1984;225:208–212.

2 Paige GD: Caloric responses after horizontal canal inactivation. Acta Otolayngol 1985;100:321–327.

3 Harada Y, Ariki T, Suzuki M: A new theory on thermal endolymphatic flow; in Graham MD, Kemink JL (eds): The Vestibular System: Neurophysiologic and Clinical Research. New York, Raven Press, 1987, pp 107–114.

4 Suzuki M, Kadir A, Hayashi N, Takamoto M: Direct influence of temperature on the semicircular canal receptor. J Vestib Res 1998;8:169–173.

5 Arai Y, Yakushin SB, Cohen B, Suzuki J, Raphan T: Spatial orientation of caloric nystagmus in semicircular canal-plugged monkeys. J Neurophysiol 2002;88:914–928.

6 Milhaud PG, Pondugula SR, Lee JH, Herzog M, Lehoueller J, Wangemann P, Sans A, Marcus DC: Chloride secretion by semicircular canal duct epithelium is stimulated via beta 2-adrenergic receptors. Am J Physiol Cell Physiol 2002;283:C1752–C1760.

7 Vosteen KH: Formation of the inner ear lymphs: permeability of ear membranes. Arch Otorhinolaryngol 1976;212:219–229.

8 Suzuki J: Selective canal plugging in monkeys. Practica Otorhinolaryngol 1994;87:1171–1180.

9 Ferry E, Bernard C, Oudar O, Sterkers O, Amiel C: Secretion of endolymph by the isolated frog semicircular canal. Acta Otolaryngol 1992;112:294–298.

Available online at www.sciencedirect.com
ScienceDirect
Neuroscience Letters 406 (2006) 1–5
Neuroscience Letters
www.elsevier.com/locate/neulet

Axonal pathways and projection levels of anterior semicircular canal nerve-activated vestibulospinal neurons in cats

Naoharu Kitajima [a,b,*], Akemi Sugita-Kitajima [a,c], Rishu Bai [a], Mitsuyoshi Sasaki [a], Hitoshi Sato [a], Midori Imagawa [a], Eiichi Kawamoto [d], Mamoru Suzuki [b], Yoshio Uchino [a]

[a] *Department of Physiology, Tokyo Medical University, 6-1-1 Shinjuku, Shinjuku-ku, Tokyo 160-8402, Japan*
[b] *Department of Otolaryngology, Tokyo Medical University, 6-7-1 Nishishinjuku, Shinjuku-ku, Tokyo 160-0023, Japan*
[c] *Department of Otolaryngology, St. Marianna University School of Medicine, 2-16-1 Sugao, Miyamae-ku, Kawasaki, Kanagawa 216-8511, Japan*
[d] *Animal Research Center, Tokyo Medical University, 6-1-1 Shinjuku, Shinjuku-ku, Tokyo 160-8402, Japan*

Received 9 January 2006; received in revised form 30 May 2006; accepted 11 June 2006

Abstract

Using collision tests of orthodromically and antidromically generated spikes, we studied the axonal pathways, axonal projection levels, and soma location of anterior semicircular canal (AC) nerve-activated vestibulospinal neurons in decerebrate cats. AC nerve-activated vestibulospinal neurons ($n = 74$) were mainly located in the ventral portion of the lateral vestibular nuclei and the rostral portion of the descending vestibular nucleus, which is consistent with previous studies. Of these neurons, 15% projected through the ipsilateral (i-) lateral vestibulospinal tract (LVST), 74% projected through the medial vestibulospinal tract (MVST), and 11% projected through the contralateral (c-) LVST. The vast majority (78%) of AC nerve-activated vestibulospinal neurons were activated antidromically only from the cervical segment of the spinal cord; 15% of neurons were activated from the T1 segment and only one neuron was activated from the L3 segment. AC nerve-activated vestibulospinal neurons may primarily target the neck muscles and thus contribute to the vestibulocollic reflex. Most of the c-LVST neurons were also activated antidromically from the oculomotor nucleus, suggesting that they are closely related to the control of combined eye-head movements.

Keywords: Anterior semicircular canal; Vestibulospinal reflex; Vestibulospinal tract; Vestibuloocular reflex; Head movement

The vestibular organs, which consist of three orthogonal semicircular canals (anterior, horizontal, and posterior) and two otolith organs (utricle and saccule) in mammals, provide important inputs involved in detecting head movements. These vestibulospinal pathways have been investigated using electrophysiological [2,5,14,17,19–22,25] and anatomical methods using horseradish peroxidase [3,4]. Activation of afferents from these receptors evokes vestibulospinal and vestibuloocular reflexes. Our previous work determined the main projection features of utricular (UT) nerve-, saccular (SAC) nerve-, and horizontal semicircular canal (HC) nerve-activated vestibulospinal neurons [12,13,16]. The majority of axons from UT nerve-activated vestibulospinal neurons descend through the ipsilateral (i-) lateral vestibulospinal tract (LVST); the axons of 14% of these neurons descend as far as the lumbar segment [12,13]. On the other hand, the axons of 63% of SAC nerve-activated vestibulospinal neurons descend through the medial vestibulospinal tract (MVST); the axons of 7% of these neurons reach as far as the lumbar spinal cord [12,13]. Most axons from HC nerve-activated vestibulospinal neurons descend through the MVST, and almost all of these axons reach cervical levels of the spinal cord [16].

The present study was designed to clarify the location, projection level and axonal pathway(s) of anterior semicircular canal (AC) nerve-activated vestibular neurons, and to elucidate the functional similarities and differences between AC nerve-activated vestibular neurons and HC nerve- or otolith-activated vestibular neurons in controlling the vestibulospinal reflex. One prior anatomical study showed that vestibulospinal neurons send descending axons through the contralateral (c-) LVST as well as through the i-LVST and MVST [11,12]. Thus far, however, one electrophysiological study suggested that HC nerve-activated vestibulospinal neurons do not send axons through the c-LVST

* Corresponding author at: Department of Otolaryngology, Tokyo Medical University, 6-7-1 Nishishinjuku, Shinjuku-ku, Tokyo 160-0023, Japan.
Tel.: +81 3 3342 6111.
E-mail address: medart@js6.so-net.ne.jp (N. Kitajima).

0304-3940/$ -- see front matter © 2006 Elsevier Ireland Ltd. All rights reserved.
doi:10.1016/j.neulet.2006.06.024

[16]. Whether AC nerve-activated vestibulospinal neurons project through this tract is another interest of the present study. Preliminary results were reported previously in abstract form [7].

Experiments were performed on eight adult cats in conformity with *The Guiding Principles for the Care and Use of Animals in the Field of Physiological Sciences*, The Physiological Society of Japan, 1988. Cats weighed between 3 and 4 kg. All animals were initially anesthetized with ketamine hydrocholoride (Ketalar, 50 mg/kg, i.m.; Parke-Davis) and later by halothane-nitrous oxide inhalation after a tracheotomy was performed. During the last stage of surgery, all cats were decerebrated at the precollicular level and prepared for recording without anesthesia. They were paralyzed by intravenous administration of pancuronium bromide (Mioblock, 0.25–0.5 mg/kg/h; Organon) and were ventilated artificially. To ensure a stable and painless condition, we monitored the depth of anesthesia frequently by observing pupil dilation. Mean arterial pressure was monitored routinely from the femoral artery. When necessary, 5–10% glucose was administered intravenously to maintain arterial pressure at 100–130 mmHg. Body temperature was maintained at around 37.5 °C with a heating pad.

The procedures for selectively stimulating the AC nerve have been described elsewhere [18,19]. The ampullary nerves of the horizontal semicircular canal and otolith nerves were transected at the inner ear and retracted. Two silver bipolar electrodes (acupuncture needles; inter-electrode distance of approximately 0.8 mm; insulated except for 150–500 μm at tips) were placed within the AC nerve of the left inner ear. Optimum electrode position for stimulating the AC nerve was determined by monitoring the cats for characteristic upward eye movements during repetitive stimulation [18]. To avoid nerve desiccation and stimulus current spread, the AC nerve and the tips of the electrodes were covered with a semisolid paraffin-Vaseline mixture. The inner ear was drained of fluid using small twisted cotton swabs, and electrodes were fixed to the occipital bone with dental cement. Cathodal current pulses of 150 μs duration were applied to the AC nerve at a rate of 2–2.5 Hz. At the beginning of each recording session, we checked the validity of selective stimulation by recording field potentials in the lateral vestibular nucleus. Stimulation of the AC nerve evoked a small positive P wave and a negative N1 potential, which resulted from the arrival of afferent impulses and monosynaptic activation of second-order vestibular neurons [9]. The amplitude of the N1 field potentials increased as the stimulus intensity increased, then reached a plateau at a stimulus intensity of about four to six times the N1 threshold (N1T). This plateau represents the maximum activation of the AC nerve [23,24,26]. With increasing stimulation, the amplitude again increased above the plateau, which indicated that stimulus current had spread to other nerves. We stimulated the AC nerve at intensities below or at the plateau level of the N1 field potential amplitudes to avoid current spread to the other vestibular nerves.

We positioned a bipolar electrode into the oculomotor nucleus to determine whether AC nerve-activated vestibular neurons send ascending axonal branches to the oculomotor nucleus. Before paralyzing the cat with pancuronium bromide, we checked for eye movements evoked by electric stimulation, indicating that the electrode was positioned correctly within the oculomotor nucleus.

Surgical and stimulating procedures for the spinal cord were as described by Rapoport et al. [10]. Laminectomies were made at the C1/C2 junction and the C3, T1, and L3 segments to place electrodes for antidromic stimulation of vestibulospinal neuron axons. Monopolar silver electrodes were used for stimulation of the spinal cord. Three electrodes were inserted into the C1/C2 junction to stimulate the MVST, i-LVST, and c-LVST. For the i-LVST and c-LVST, electrodes were placed approximately 2.5 mm lateral to midline on the left and right sides, while for the MVST, an electrode was placed near the midline. Three pairs of electrodes were positioned bilaterally in the upper cervical segments (C3), near the cervical enlargement (T1), and in the upper lumbar segment (L3) to antidromically activate vestibulospinal neurons. All electrodes were positioned at locations that elicited low-threshold antidromic field potentials in the vestibular nuclei. Placement of all electrodes was performed while recording antidromic field potentials in the lateral vestibular nucleus. We concluded that a neuron did not project through the spinal cord if an antidromic response could not be elicited in that neuron after delivering a strong stimulus current to the spinal cord (i.e., more than 1 mA, typically 2–5 mA).

Field potentials and extracellular single-unit potentials were recorded in the left vestibular nuclei with glass micropipettes containing 2 M NaCl solution saturated with Fast green dye. Projections of the AC nerve-activated vestibulospinal neurons were confirmed by observing whether action potential collisions occurred between orthodromically and antidromically generated action potentials. Axonal pathways were determined by antidromic stimulation at the C1/C2 junction. We classified an axon as traveling in the LVST or MVST only when it was excited by stimulation from a single electrode or when the threshold difference among effective electrodes exceeded 3:1 [1]. Conduction velocities in the spinal cord were calculated from measuring the latency difference between the C1/C2 junction and T1 if neurons were activated from T1; otherwise they were calculated from those between the C1/C2 junction and C3. If the C3 segment was not activated, we did not calculate the conduction velocity, because the distance from the vestibular nuclei to the C1/C2 junction was too short to estimate the conduction velocity by electrophysiological means. The recording sites of field potentials and unit activities in the vestibular nuclei were marked with a dye injection. At the end of each experiment, a lethal dose of anesthetic was administered, and the brain stem and stimulated spinal segments were removed and fixed in 10% formalin solution. Frozen serial sections (100 μm thick) were cut transversely and Nissl stained. We used these sections to identify the recording and stimulating sites.

We recorded 85 vestibular neurons that were activated by stimulation of the AC nerve. These neurons could be classified into three groups according to their axonal projections [4,5]. The first group of neurons, termed vestibulospinal (VS) neurons, sent their axons to the spinal cord but not to the oculomotor nucleus. The second group of neurons, termed vestibulooculospinal (VOS) neurons, sent axon collaterals to both the oculomotor nucleus and the spinal cord. The third group of neurons,

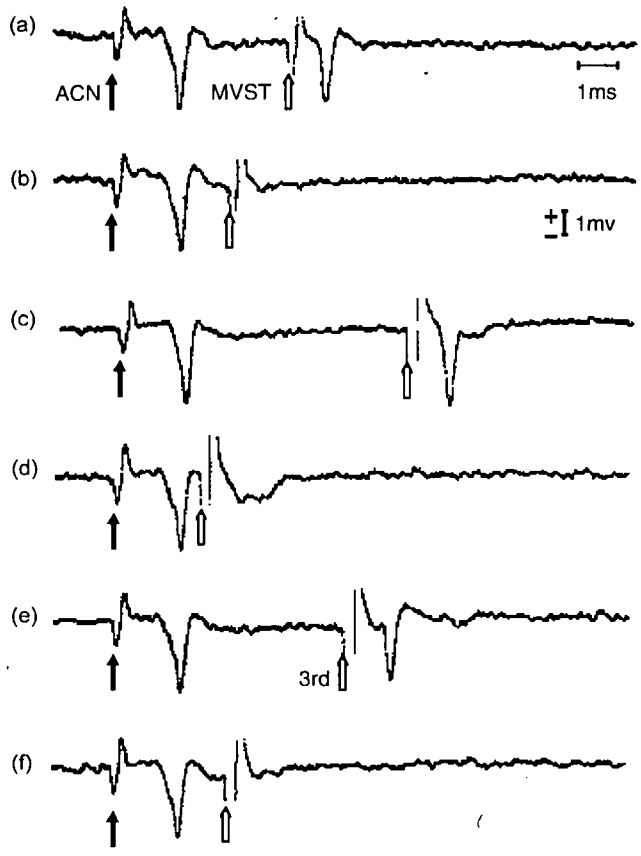

Fig. 1. Example of an AC nerve-activated VOS neuron. (a) Stimulation of the AC nerve at 5 μA (solid arrow) elicited an orthodromic spike in this neuron. This neuron was also activated antidromically from the MVST at the C1/C2 junction at 100 μA (small open arrow). (b) The antidromic spike elicited by C1/C2 stimulation collided with a preceding orthodromic spike elicited by AC nerve stimulation. (c) This neuron was also activated antidromically from C3 at 150 μA. (d) The antidromic spike elicited from C3 stimulation collided with a preceding orthodromic spike elicited by AC nerve stimulation. (e, f) Stimulation of the AC nerve at 5 μA evoked an orthodromic spike that collided with and blocked the antidromic spike resulting from stimulation of the oculomotor nuclei (large open arrow).

termed vestibuloocular (VO) neurons, sent their axons to the oculomotor nucleus but not to the spinal cord. Judging from the orthodromic latencies [9] 74 recorded units were second-order vestibular neurons (latency of less than 1.4 ms) and 11 were third-order vestibular neurons (latency ranged from 1.5 to 2.1 ms). These 85 neurons were classified as VS ($n = 32$), VOS ($n = 41$), and VO ($n = 12$) neurons.

Fig. 1 shows an example of a VOS neuron. Stimulation of the AC nerve evoked an orthodromic spike with a latency of 1.2 ms. The same neuron was activated antidromically after stimulation of the MVST at the C1/C2 junction (trace 1). The antidromic spike was blocked by the preceding orthodromic spike when the interval between the orthodromic spike and the antidromic stimulation was shortened to less than the latency of antidromic spikes plus the refractory period (trace 2). This neuron was also activated antidromically from the C3 segment (trace 3) and from the oculomotor nucleus (trace 5); antidromic spikes collided with preceding orthodromic spikes (traces 4 and 6). We could not elicit an antidromic response from this neuron by stimulating either T1 or L3. These firing characteristics led us to classify this neuron as an AC nerve-activated VOS neuron whose axon descended through the MVST, reaching as far as the cervical segments.

The locations of AC nerve-activated, second-order vestibular neurons in diagrams of transverse sections are shown in Fig. 2a. The vast majority of vestibulospinal neurons (VS and VOS neurons) were located in the lateral and descending vestibular nuclei, and a few were in the medial vestibular nucleus. Most of VO neurons were located in the superior nucleus. A small number of third-order neurons (5 VO, 1 VS, and 2 VOS) were also recorded. Most of them were located in the rostroventral part of the descending vestibular nucleus (not shown to avoid complication of the figure).

We identified 72 vestibulospinal neurons (VS and VOS neurons) (Table 1). The majority of these neurons sent descending axons through the MVST, while only a minority sent axons through the i- or c-LVST. The vast majority of AC nerve-activated vestibulospinal neurons projected only to the cervical segments (see Fig. 2b; open circles). A small portion of MVST neurons, a few i-LVST neurons, but no c-LVST neurons projected as far as thoracic or lumbar levels. These neurons were most frequently found at the rostral edge of the descending nucleus (closed circles). One third-order neuron that sent an axon as far as the lumbar segment was also located in the descending vestibular nucleus (not shown).

We studied the projection patterns of AC nerve-activated vestibulospinal neurons, which include VS and VOS neurons. AC nerve-activated vestibulospinal neurons were mainly located in the lateral and the descending vestibular nuclei, which is consistent with previous studies [20,21]. By stimulating the

Table 1
The type of ACN-activated vestibulospinal neurons that were activated from each spinal segment

	C1/2		C3		T1		L3	
	n	(%)	*n*	(%)	*n*	(%)	*n*	(%)
Total	72	100	57	79	11	15	1	1
i-LVST								
a	10	14	7	10	1	1	0	0
b	1	1	1	1	1	1	1	1
MVST								
a	49	68	40	56	9	13	0	0
b	4	6	3	4	0	0		
c-LVST								
a	8	11	6	8	0	0		

AC nerve-activated vestibulospinal neurons that were activated antidromically from each spinal segment. Seventy-two neurons (uppermost row; total) were divided into ipsilateral vestibulospinal tract (i-LVST), medial vestibulospinal tract (MVST), and contralateral vestibulospinal tract (c-MVST) neurons. They were further subdivided into second-order (a), and third-order (b) neurons. C, cervical segment; T, thoracic segment; L, lumbar segment. *n* refers to the number of vestibulospinal neurons that could be activated from the indicated spinal segments. The percentages refer to the total number of AC nerve-activated vestibulospinal neurons. The number and the percentage at the rostral segment include neurons that were activated from the caudal segments. a: second-order neuron; b: third-order neuron.